catalysts

MDPI

Article

Developing Multifunctional Fe-Based Catalysts for the Direct Hydrogenation of CO_2 in Power Plant Flue Gas to Light Olefins

Likui Feng [1,2], Shuai Guo [2], Zhiyong Yu [1,2], Yijie Cheng [1,2], Julan Ming [2], Xiaoning Song [2], Qiuyang Cao [2], Xiaofeng Zhu [1], Guanghui Wang [1], Di Xu [3,*] and Mingyue Ding [3,*]

1 E. Energy Technology Co., Ltd., Hangzhou 310014, China; wwwhflk@163.com (L.F.); 13575739448@163.com (X.Z.)
2 State Grid Zhejiang Electric Power Co., Ltd., Research Institute, Hangzhou 310014, China; guoshuai_12@163.com (S.G.); qycao99@163.com (Q.C.)
3 School of Power and Mechanical Engineering, Wuhan University, Wuhan 430072, China
* Correspondence: x_d@whu.edu.cn (D.X.); dingmy@whu.edu.cn (M.D.)

Abstract: The hydrogenation of carbon dioxide (CO_2) to produce light olefins is one of the most promising ways to utilize CO_2 in power plant flue gas. However, the low concentration of CO_2 (~10%) and the existence of water steam in the flue gas pose great challenges for the catalyst design. To address these problems, we introduced a Mg promoter and hydrophobic component into the Fe-based catalyst to improve the CO_2 adsorption capacity and weaken the negative effects of water. The yield of light olefins on an optimized multifunctional Fe-based catalyst increased by 37% in low-concentration CO_2 hydrogenation with water steam. A variety of characterizations proved that the Mg promoter played critical roles in regulating the adsorption capacity of CO_2, increasing the surface electron density of Fe species, and promoting the formation of iron carbide active sites. The hydrophobic component mainly contributed to constraining the oxidation of iron carbides via water steam. It benefited from the rational design of the catalyst, showing how our multifunctional Fe-based catalyst has great potential for practical application in CO_2 utilization.

Keywords: multifunctional; Fe-based catalyst; low concentration CO_2 hydrogenation; water steam; light olefins

Citation: Feng, L.; Guo, S.; Yu, Z.; Cheng, Y.; Ming, J.; Song, X.; Cao, Q.; Zhu, X.; Wang, G.; Xu, D.; et al. Developing Multifunctional Fe-Based Catalysts for the Direct Hydrogenation of CO_2 in Power Plant Flue Gas to Light Olefins. *Catalysts* **2024**, *14*, 204. https://doi.org/10.3390/catal14030204

Academic Editor: Zhong-Wen Liu

Received: 31 January 2024
Revised: 22 February 2024
Accepted: 1 March 2024
Published: 20 March 2024

1. Introduction

Since the late 20th century, various environmental problems caused by a large amount of greenhouse gases, including CO_2 emissions, have widely concerned the world. In this regard, carbon neutrality has been accepted by most countries. To achieve this goal, on the one hand, the use of fossil fuels should be reduced to decrease CO_2 emissions at the source; on the other hand, effluent CO_2 could be utilized by converting CO_2 into high-value-added chemicals [1–3]. Light olefins are important chemical raw materials that are widely used in the production of various polymeric materials and fine chemicals [4–6]. Additionally, ethylene is an important symbol to evaluate the development level of the petrochemical industry. Using CO_2 as raw material to produce light olefins is a promising way to achieve CO_2 emissions reduction and CO_2 utilization.

Catalytic hydrogenation is one of the feasible ways for CO_2 conversion to light olefins. The reaction route is as follows: CO_2 is first reduced to CO via a reverse water gas shift (RWGS) reaction, and then CO is converted to light olefins via the Fischer–Tropsch synthesis (FTS) reaction [7]. Fe-based catalysts have been extensively studied for CO_2 hydrogenation to olefins due to the dynamic matching of RWGS and FTS reactions [8–10]. For example, Sun et al. developed alkali metals and modified Fe-based catalysts for CO_2 hydrogenation to light olefins, which exhibited a CO_2 conversion of 40.5% and a light olefin selectivity of 46.6% under reaction conditions of 3 MPa and 320 °C [11]. They proposed that alkali metal additives promoted CO dissociation, thus favoring the formation of an iron carbide active

phase. Additionally, alkali metal promoters were proven to inhibit the hydrogenation of olefin intermediates, thus improving olefin selectivity. Ma et al. studied the synergistic effect of Mn and Na on Fe-based catalysts for CO_2 hydrogenation [12]. The Mn promoter was supposed to disperse and stabilize Fe species, while the Na promoter mainly acted as an electron donator. The optimized Na and Mn co-modified Fe-based catalyst exhibited the highest olefin/paraffin ratio of 8.1. For iron-based catalysts, iron oxide and iron carbide are generally considered to be the active phases of RWGS and FTS reactions, respectively [13,14]. The presence of water steam in feed gas could lead to the oxidation of iron carbide to iron oxide, resulting in a significant decrease in catalytic activity [15–17]. Introducing water-conducting or hydrophobic components has been proven to be an effective strategy to restrain the negative effect of water on catalysts [17–19]. Therefore, the rational design of the catalyst according to the reaction environment is of great importance in CO_2 hydrogenation to light olefins.

Coal-fired power generation occupies a leading position in power generation. In the meantime, coal-fired power plants emit large amounts of CO_2 each year [20–22]. Therefore, it is of great significance to make efficient use of CO_2 in flue gas. The concentration of CO_2 in the flue gas of power plants is usually about 10%, and the rest is mostly made up of N_2 [23–25]. Traditional CO_2 catalytic hydrogenation uses high-purity CO_2 as a raw material, which faces the problem of high capture costs [26–28]. Based on that, the direct use of plant flue gas containing low-concentration CO_2 as raw material to prepare light olefins has potential economic benefits. Additionally, the effects of water steam in flue gas on the catalyst and reaction should not be ignored. Developing highly active Fe-based catalysts for the conversion of CO_2 in flue gas has great significance but results in a big challenge. Herein, we designed and prepared a multifunctional Fe-based catalyst with Mg as the promoter and polydivinylbenzene (PDVB) as the hydrophobic component for converting CO_2 in flue gas into light olefins. The optimized multifunctional catalyst achieved a CO_2 conversion of 25.2% and a light olefin yield of 5.47% for H_2O-containing low-concentration CO_2 hydrogenation. The effects of Mg doping and hydrophobic PDVB introduction on catalytic performance and the internal regulatory mechanism were studied. This could accumulate theoretical knowledge for the development of catalysts in H_2O-containing low-concentration CO_2 hydrogenation to light olefins with industrial application prospects.

2. Results and Discussion

2.1. CO_2 Hydrogenation Performance under Simulant Power Plant Flue Gas Conditions

The prepared $KFMM_x$ were generally tested for CO_2 hydrogenation at 320 °C, 3 MPa, and 4000 mL/(g_{cat}·h) with a CO_2 content of 10%. As shown in Figure 1a,b, the CO_2 conversion produced a volcanic curve with a Mg doping amount and peaked at 25.2% when the molar ratio of Mg/Fe was 0.15. Therefore, with the addition of Mg, CO selectivity decreased to a certain extent, indicating the accelerated conversion of CO_2 to hydrocarbons via the CO intermediate [7]. Light olefins selectivity and the olefins/paraffin (o/p) ratio both increase after doping Mg, suggesting the promotion effect of Mg on olefin synthesis. Among the $KFMM_x$ catalysts, $KFMM_{0.15}$ shows the best performance with a CO_2 conversion of 25.2%, a light olefins selectivity of 24.7%, and an o/p ratio of 4.33. The light olefins yield of $KFMM_{0.15}$ reached 6.22%, which is 38.8% higher than that of the undoped Mg catalyst (4.48%). All these results prove that the introduction of appropriate Mg is conducive to the conversion of low-concentration CO_2 to light olefins. The effects of the reaction temperature and weight hour space volume (WHSV) on the light olefin synthesis of $KFMM_{0.15}$ were further studied. As shown in Figure 1c,d, high temperature favored the conversion of CO_2, but the light olefin selectivity and o/p ratio both decreased. As there is a reduction in WHSV, the yield of light olefins clear improves to 7.68% due to the accelerated conversion of CO_2 to 33.1%, with light olefin selectivity stabilizing at around 23%.

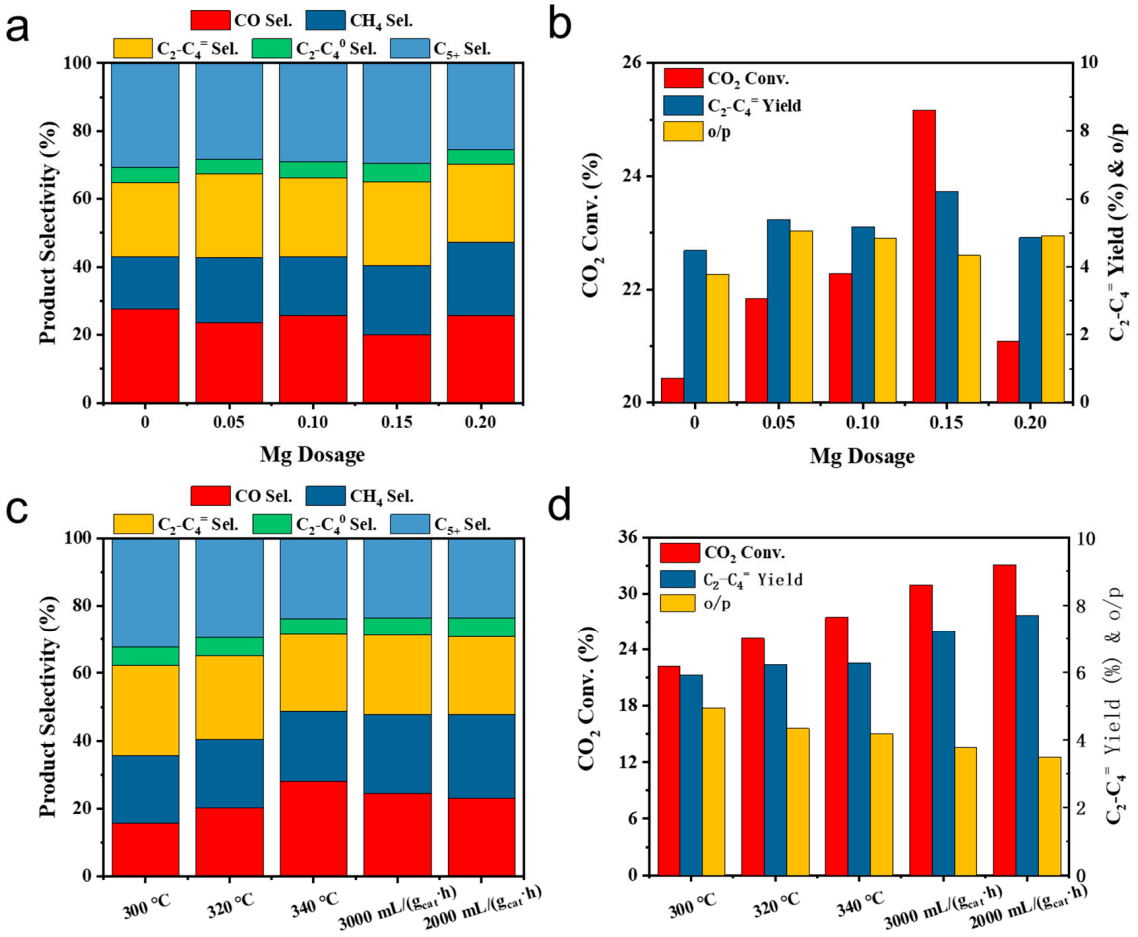

Figure 1. (**a**,**b**) Catalytic performance of $KFMM_X$ catalysts. Reaction conditions: $CO_2/H_2/N_2 = 10/30/60$, 320 °C, 3 MPa, and 4000 mL/(g_{cat}·h). (**c**,**d**) Effect of reaction temperatures and pressures on catalytic performance over $KFMM_{0.15}$.

Considering that the flue gas contains water steam, we further introduced water steam in reactant gas to study the effect of water steam on light olefin synthesis. The catalytic performances were tested at 340 °C, 3 MPa, and 4000 mL/(g_{cat}·h) with a CO_2 content of 10% and water steam content of 4%. As shown in Figure 2a,b, the addition of water had a significantly negative effect on catalytic performance. Specifically, the CO_2 conversion decreased from 33.1% to 20.5%, and the CO selectivity increased from 22.9% to 42.1%. Although the light olefin selectivity slightly increased to 33.7%, the yield of light olefins was significantly reduced from 7.68% to 3.99%. In order to weaken the negative effect of water steam, we introduced hydrophobic PDVB to construct composite catalysts. As for composite catalysts with the powder mixing of $KFMM_x$ and PDVB ($KFMM_x$/PDVB-P), the conversion of CO_2 increases to 25.2%, and the selectivity of CO decreases to 31.9% compared to $KFMM_x$ alone, indicating the promoted conversion of CO_2 via CO. Moreover, the yield of light olefins increased to 5.47%, which is 36.9% higher than that of $KFMM_x$. We speculate that the addition of hydrophobic PDVB could avoid sufficient contact between the water steam and the catalyst surface, thus weakening the oxidation effect of H_2O on the catalyst. However, when $KFMM_x$ is mixed with PDVB by mortar mixing ($KFMM_x$/PDVB-M), the catalytic performance is severely weakened. Specifically, the CO_2 conversion and CO selectivity on $KFMM_x$/PDVB-M are 15.2% and 78.8%, respectively. The selectivity and yield of light olefins are as low as 19.8% and 0.64%. In addition, the catalytic performance of granule mixing for the composite catalyst ($KFMM_x$/PDVB-G) is between the above two catalysts. This reminds us that the distance between $KFMM_x$ and PDVB is critical to light olefin synthesis, and $KFMM_x$/PDVB-P shows the best catalytic performance in H_2O-

containing low-concentration CO_2 hydrogenation. More than that, we further studied the effect of H_2O dosage. As shown in Figure 2c,d, the yield of CO_2 conversion and light olefins both decreased with the increase in H_2O dosage, while the H_2O dosage had little effect on light olefin selectivity. The optimized $KFMM_x$/PDVB-P catalyst exhibited good stability even in a water steam atmosphere (Figure 2e). In summary, optimized $KFMM_x$/PDVB-P exhibited great potential in CO_2 hydrogenation to light olefins under simulant flue gas conditions compared to conventional Fe-based catalysts.

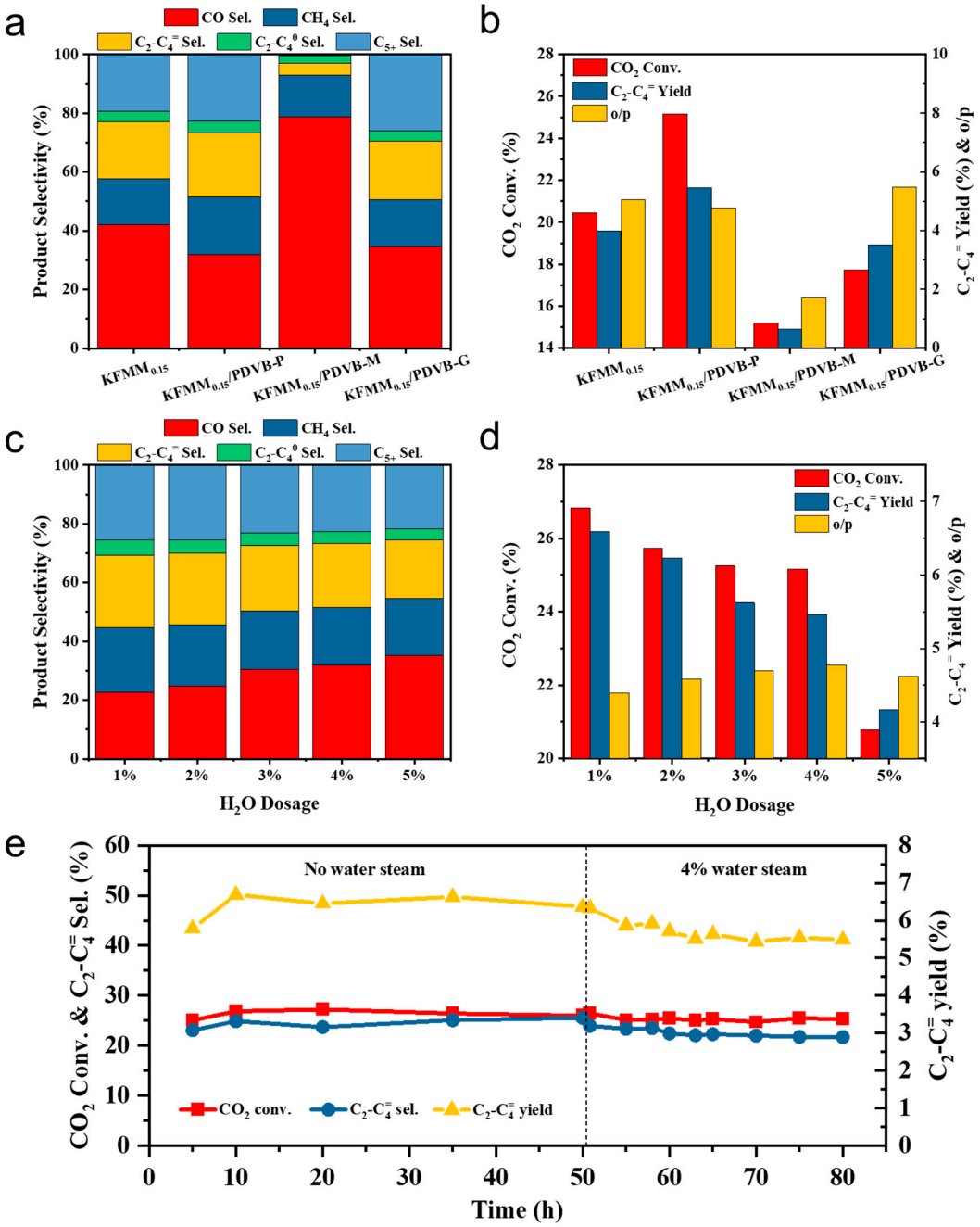

Figure 2. (**a**,**b**) Catalytic performance of $KFMM_{0.15}$/PDVB catalysts with different stacking manners. Reaction conditions: $CO_2/H_2/N_2/H_2O$ = 9.6/28.8/57.6/4, 340 °C, 3 MPa, and 4000 mL/(g_{cat}·h). (**c**,**d**) Effect of water steam dosage on catalytic performance over the $KFMM_{0.15}$/PDVB-P catalyst. (**e**) Stability test of $KFMM_{0.15}$/PDVB-P catalyst. Reaction conditions: $CO_2/H_2/N_2$ = 10/30/60 or $CO_2/H_2/N_2/H_2O$ = 9.6/28.8/57.6/4, 340 °C, 3 MPa, and 4000 mL/(g_{cat}·h).

2.2. Structural Characterization

The N_2 absorption–desorption isotherms of series $KFMM_x$ catalysts are shown in Figure 3a. All these catalysts exhibit type IV isotherms with hysteresis belonging to type H2b, indicating the complex porous structure. In addition, the BET-specific surface area of $KFMM_x$ catalysts improves with the introduction of Mg (Table 1). Specifically, the BET-specific surface area of $KFMM_{0.15}$ is 82 m^2/g, which is 1.7 times that of $KFMM_0$ (48 m^2/g). The pore size distributions of $KFMM_x$ catalysts clearly confirm the newly emerged mesoporous with a pore size of around 13 nm (Figure 3b). The increased BET-specific surface area and newly emerged mesoporous structure after introducing Mg are due to the pore-forming effect of carbonate decomposition during calcination, which is conducive to the adsorption of reactant molecules and has positive effects on catalytic performance.

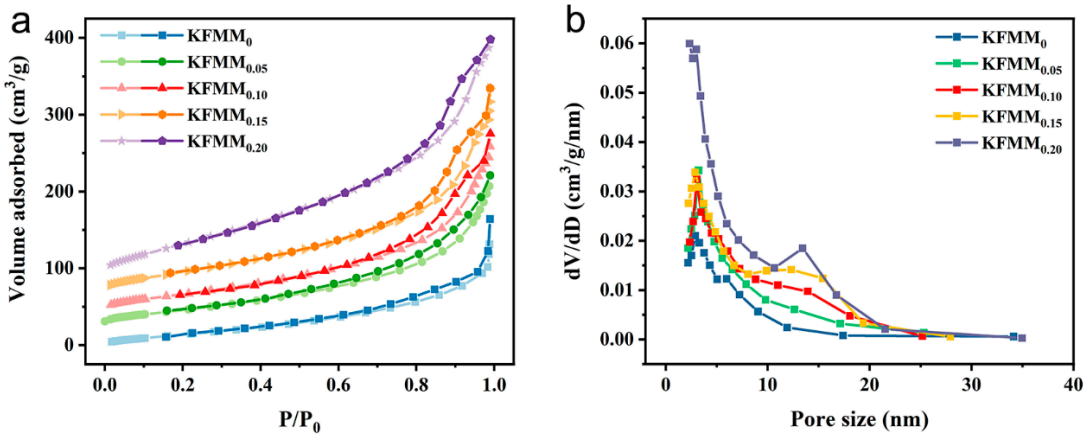

Figure 3. (**a**) N_2 adsorption–desorption isotherms and (**b**) pore size distributions of series $KFMM_x$ catalysts.

Table 1. Textual properties of $KFMM_x$ catalysts.

Catalysts	Element Contents (%)				BET Specific Surface Area (m^2/g)	Total Pore Volume (cm^3/g)
	Fe	Mn	Mg	K		
$KFMM_0$	73.9	22.5	-	3.6	47.6	0.25
$KFMM_{0.05}$	71.3	21.7	3.5	3.6	70.6	0.30
$KFMM_{0.10}$	68.6	21.3	6.8	3.3	68.7	0.35
$KFMM_{0.15}$	66.1	20.7	9.7	3.5	81.8	0.40
$KFMM_{0.20}$	64.6	20.0	12.1	3.3	145.7	0.46

The SEM images of $KFMM_0$ and $KFMM_{0.15}$ catalysts are shown in Figure 4. Figure 4a shows that $KFMM_0$ is dominated by uniform nanoparticles with a particle size of about 100 nm. By contrast, the dispersion of $KFMM_{0.15}$ is very uneven (Figure 4b). The SEM images of spent $KFMM_{0.15}$ catalysts are shown in Figure 4c. It can be found that the morphology of $KFMM_{0.15}$ is almost unchanged after the CO_2 hydrogenation reaction.

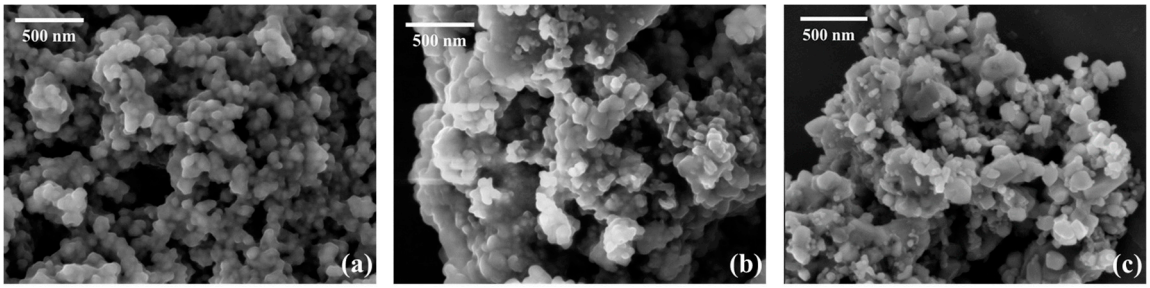

Figure 4. SEM images of (**a**) fresh $KFMM_0$, (**b**) fresh $KFMM_{0.15}$, and (**c**) spent $KFMM_{0.15}$ catalysts.

The bulk phase structures of the catalysts were studied using XRD. As shown in Figure 5a, the diffraction peaks at 30.0°, 35.4°, 43.0°, 56.9°, and 62.5° are attributed to (220), (311), (400), (511), and (440) planes of Fe_3O_4, which is the active phase of the RWGS reaction [13,14,29]. No diffraction peaks attributed to MnO and MgO appeared on fresh $KFMM_x$ catalysts, indicating good dispersion. As for the catalysts after the CO_2 catalytic hydrogenation reaction, the phase structures clearly changed. As shown in Figure 5b, the appearance of diffraction peaks at 40~46° indicates the formation of Fe_5C_2, which is the active phase of the FTS reaction [30]. In addition, the diffraction peaks at 24.6°, 31.7°, and 51.9° belong to $MnCO_3$, suggesting the phase change in MnO to $MnCO_3$ during CO_2 hydrogenation. As for $KFMM_{0.15}$/PDVB composite catalysts, the broad peak at around 20° was assigned to the amorphous structure of PDVB (Figure 5c). The XRD patterns of catalysts after the H_2O-containing CO_2 hydrogenation reaction are shown in Figure 5d. It can be found that the peak intensity of Fe_5C_2 species decreased significantly after introducing H_2O, indicating the oxidation effect of H_2O on Fe_5C_2. This is strongly related to the weakened catalytic activity. As for $KFMM_{0.15}$/PDVB-P, the peak intensity of Fe_5C_2 species was greater than the sole $KFMM_{0.15}$. This proves that the introduction of PDVB can reduce the oxidation effect of H_2O on Fe_5C_2, maybe by avoiding sufficient contact between the water steam and $KFMM_{0.15}$ surface. Moreover, the Fe_5C_2 species is almost absent, and Fe_3O_4 is the only Fe phase on $KFMM_{0.15}$/PDVB-M. This suggests that the close distance between $KFMM_{0.15}$ and PDVB could restrain the transformation of Fe_3O_4 to Fe_5C_2, thus exhibiting high CO selectivity. In summary, Fe_3O_4 and Fe_5C_2 undergo catalytic CO_2 hydrogenation to light olefins by coupling RWGS and FTS reactions. The existence of H_2O in feed gas goes against the formation of Fe_5C_2, resulting in lower activity. The introduction of hydrophobic PDVB was found to weaken the oxidation effect of H_2O and make the formation of Fe_5C_2 available. Note that a moderate distance between $KFMM_{0.15}$ and PDVB is crucial to ensure the quick removal of H_2O and avoid the negative effect of PDVB. Based on this, the $KFMM_{0.15}$/PDVB-P exhibits the best catalytic performance in H_2O-containing low-concentration CO_2 hydrogenation.

The contact angle test is performed to confirm the hydrophobic properties of the catalyst. As shown in Figure 6, the addition of PDVB can effectively increase the hydrophobicity from 66.13° to 125.21° for $KFMM_{0.15}$/PDVB-P and to 123.39° for $KFMM_{0.15}$/PDVB-M, which helps to speed up the discharge of H_2O from the catalyst surface. Moreover, the catalyst remains hydrophobic even after the catalytic reaction, indicating the good stability of PDVB during the CO_2 hydrogenation reaction. The retention of characteristic peaks of PDVB after the catalytic test further confirms its good stability (Figure 6g) [31]. Note that the retention of hydrophobicity of $KFMM_{0.15}$/PDVB-P and $KFMM_{0.15}$/PDVB m implies that the great difference in catalytic performance has nothing to do with hydrophobicity but is related to the iron phase.

XPS is used to analyze the electronic structure of catalysts. Figure 7a shows the Fe2p spectra of fresh $KFMM_0$ and $KFMM_{0.15}$ samples, in which 710.2~710.4 eV and 711.8~712.0 eV are attributed to Fe^{2+} and Fe^{3+}, respectively [30,32]. After Mg is added, all peaks shift at 0.2 eV to a lower binding energy, indicating the electron transfer from Mg to Fe. The increased electron density on the surface of iron species can facilitate the activation of CO_2 and CO molecules on the one hand, thus accelerating the conversion of CO_2 and CO [33]. On the other hand, it can inhibit the hydrogenation reaction and facilitate the desorption of olefins, thus favoring the formation of olefin products [34]. Figure 7b shows the Fe2p spectra of spent samples in which 707.8~708.3 eV is attributed to FeC_x [33,34]. Compared with the $KFMM_0$ catalyst, the relative content of FeC_x in $KFMM_{0.15}$ is higher, indicating that the addition of Mg is conducive to the formation of the FeC_x active phase. This can be reasoned by the facilitation of the CO dissociation on the electron-rich Fe surface [34,35]. Figure 7c shows the C1s spectra of spent samples. The peaks at 283.5~283.7 eV are attributed to the FeC_x species, which is consistent with the Fe2p spectra [36]. In addition, the peaks at 289.0~289.1 eV and 288.1 eV belong to carbonate and formate, both of which are important intermediates in the process of CO_2 hydrogenation [9,37,38]. Note

that the surface of $KFMM_{0.15}$ contains more carbonate species, indicating that the addition of Mg can enrich CO_2 on the catalyst surface. This enrichment effect of Mg is conducive to the adsorption and activation of CO_2 at a low concentration. As shown in Figure 7d, the introduction of water steam in feed gas leads to a decrease in the iron carbide fraction from 9.46% to 8.05%, while the introduction of PDVB increases the iron carbide fraction to 8.93%. These results indicate that water steam is not conducive to the formation of the iron carbide active phase, which is consistent with XRD results. And the introduction of PDVB could weaken the negative effect of water steam on active phase formation by avoiding prolonged contact between the water and the catalyst.

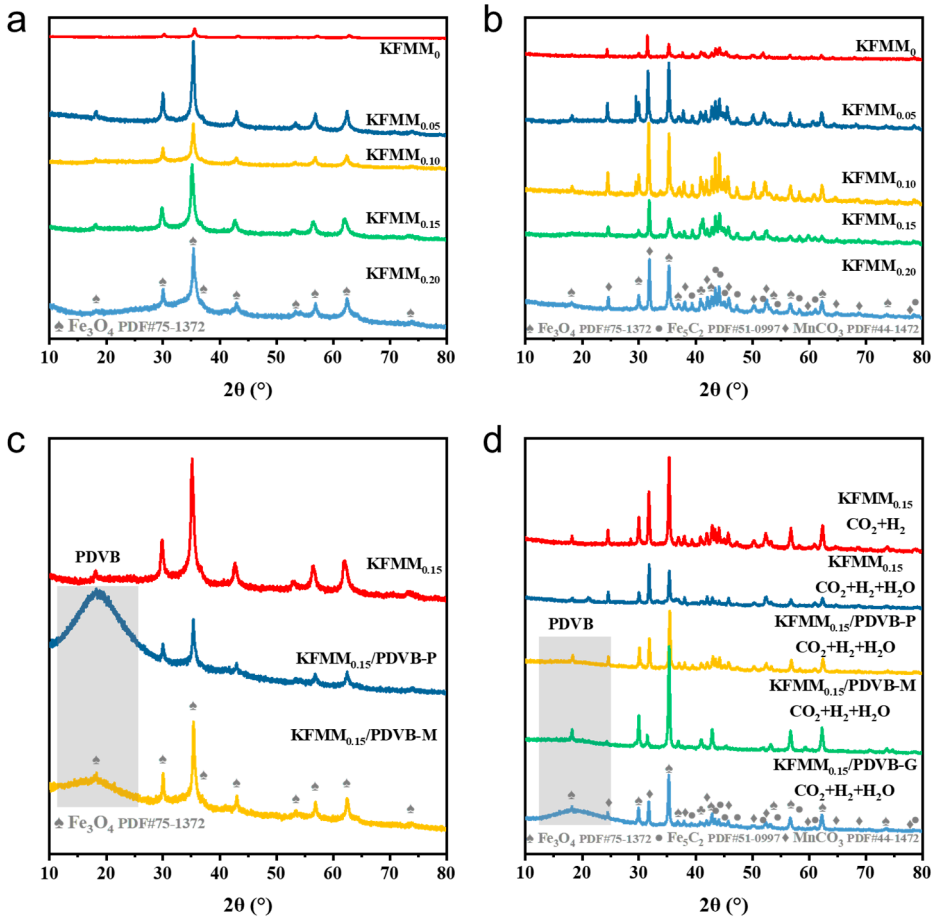

Figure 5. XRD patterns of (**a**) fresh and (**b**) spent $KFMM_x$ catalysts, (**c**) fresh. and (**d**) spent $KFMM_{0.15}$/PDVB catalysts.

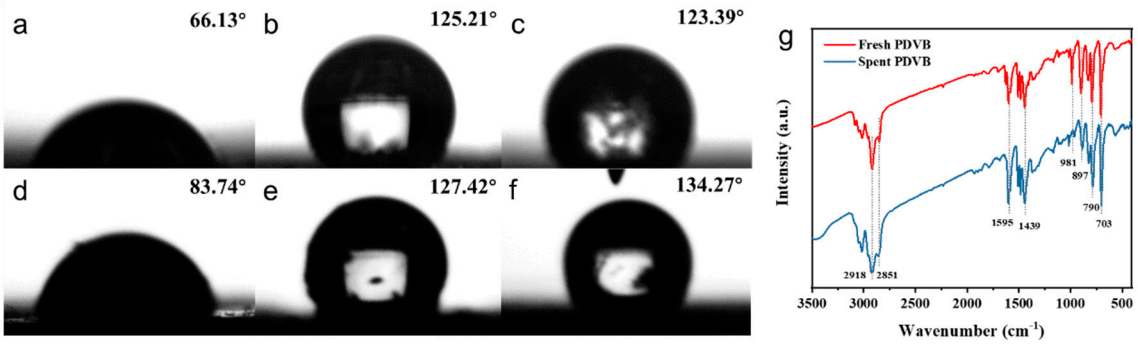

Figure 6. The contact angle of (**a**) fresh and (**d**) spent $KFMM_{0.15}$ catalysts, (**b**) fresh and (**e**) spent $KFMM_{0.15}$/PDVB−P catalysts, and (**c**) fresh and (**f**) spent $KFMM_{0.15}$/PDVB−M catalysts. (**g**) FT-IR spectra of fresh and spent PDVB.

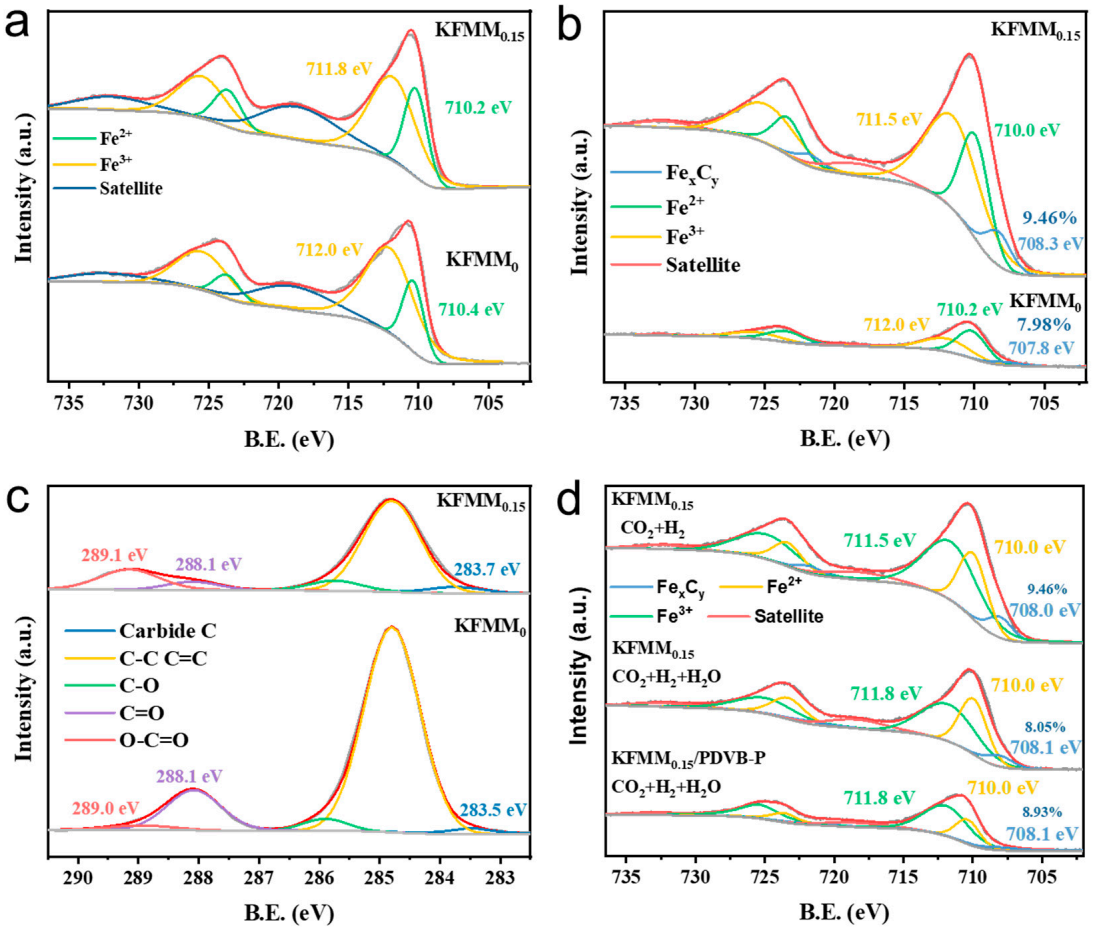

Figure 7. XPS spectra of Fe2p of (**a**) fresh and (**b**) spent $KFMM_x$ catalysts, (**c**) the C1s of spent $KFMM_x$ catalysts, and (**d**) Fe2p of spent $KFMM_{0.15}$ and $KFMM_{0.15}$/PDVB-P catalysts under $CO_2/H_2/H_2O$ atmosphere.

The H_2-TPR results of $KFMM_0$ and $KFMM_{0.15}$ catalysts are shown in Figure 8a. Three reduction peaks were observed in the temperature range of 300~800 °C, which reflected the gradual reduction process of Fe_3O_4 to metallic Fe. Among them, the reduction peak at 300~400 °C was attributed to a reduction in the Fe_3O_4 surface, while the reduction peaks at 500~550°C and after 600°C were attributed to a reduction in bulk Fe_3O_4. With the addition of the Mg promoter, the reduction in the Fe_3O_4 surface shifted to a high temperature by 40 °C, while the reduction in bulk Fe_3O_4 shifted to a low temperature by 31 °C. Moreover, the fraction reduction peak at 300~400 °C in $KFMM_{0.15}$ was greater than $KFMM_0$, indicating the promotion effect of Mg on catalyst reduction. The CO_2-TPD results of the $KFMM_0$ and $KFMM_{0.15}$ catalysts are shown in Figure 8b. There are three CO_2 desorption peaks corresponding to weakly adsorbed CO_2 (α) below 200°C, moderately strongly adsorbed CO_2 (β) at 200~500 °C, and strongly adsorbed CO_2 (γ) above 550 °C [39,40]. It was found that the addition of Mg slightly weakened CO_2's adsorption strength, leading to the desorption temperature (325 °C) being closer to the reaction temperature (320 °C). We can conclude that the addition of the Mg promoter could optimize the CO_2 adsorption capacity of the catalyst and is more conducive to the activation of CO_2.

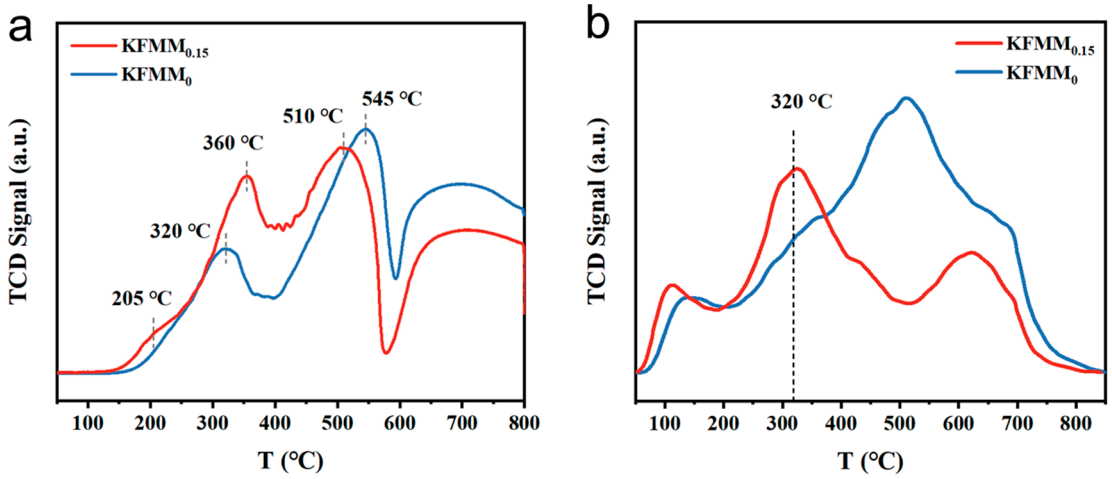

Figure 8. (**a**) H_2-TPR and (**b**) CO_2-TPD results of $KFMM_0$ and $KFMM_{0.15}$ catalysts.

2.3. Reaction Mechanism Study

We further performed in situ CO_2 hydrogenation DRIFTS tests to study the reaction mechanism on $KFMM_0$ and $KFMM_{0.15}$ catalysts. As shown in Figure 9a,b, as for the $KFMM_0$ catalyst, the IR bands at 2954/2932/2855/2723/1618/1374 cm^{-1}, assigned to the formate intermediate (*HCOO), appeared rapidly with the introduction of CO_2/H2 [41,42]. In addition, weak signals attributed to gaseous CO (2220~2050 cm^{-1}) and linearly adsorbed CO (2075 cm^{-1}) also appeared [43–46]. With the extension of the reaction time, the peak intensity of the above adsorbates was almost unchanged, and no CH_4 was detected. This suggests that the subsequent conversions of intermediates to hydrocarbons are difficult in the $KFMM_0$ catalyst. As for the $KFMM_{0.15}$ catalyst (Figure 9c,d), a carbonate (*CO_3^{2-}, 1500/1268 cm^{-1}) species was observed, indicating CO_2's stronger adsorption ability, which is consistent with the XPS and CO_2-TPD results [47,48]. More than that, the formation rate of the CO species was much faster than $KFMM_0$. This reminds us that improved CO_2 adsorption favors the formation of CO species. In addition, the gaseous CH_4 product (3015 cm^{-1}) was detected as the reaction continued [39,49]. We speculate that the CO species was the intermediate of CH_4 formation, while the formate acted as a spectator in our catalyst [50,51]. We conclude that the introduction of Mg promotes CO_2 adsorption and the RWGS reaction, thus accelerating the subsequent conversion of the CO intermediate to light olefins.

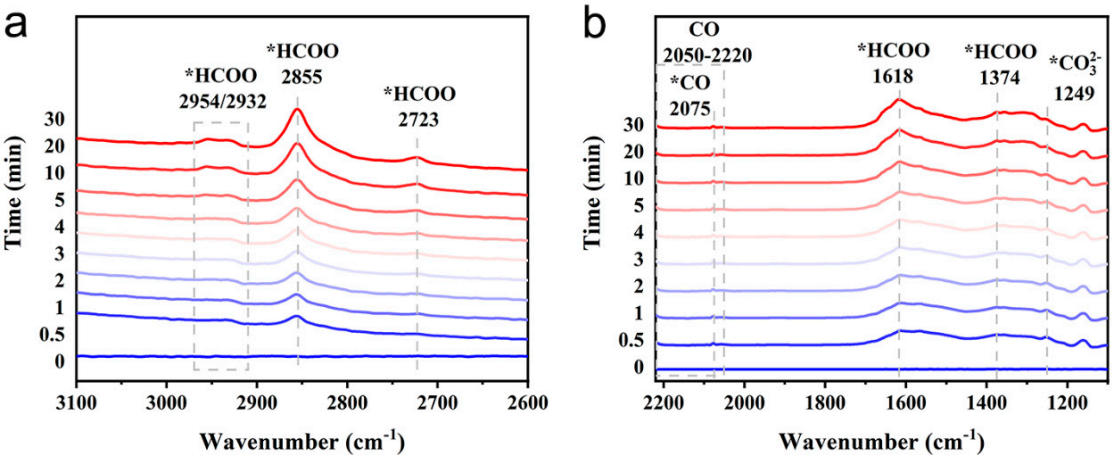

Figure 9. *Cont.*

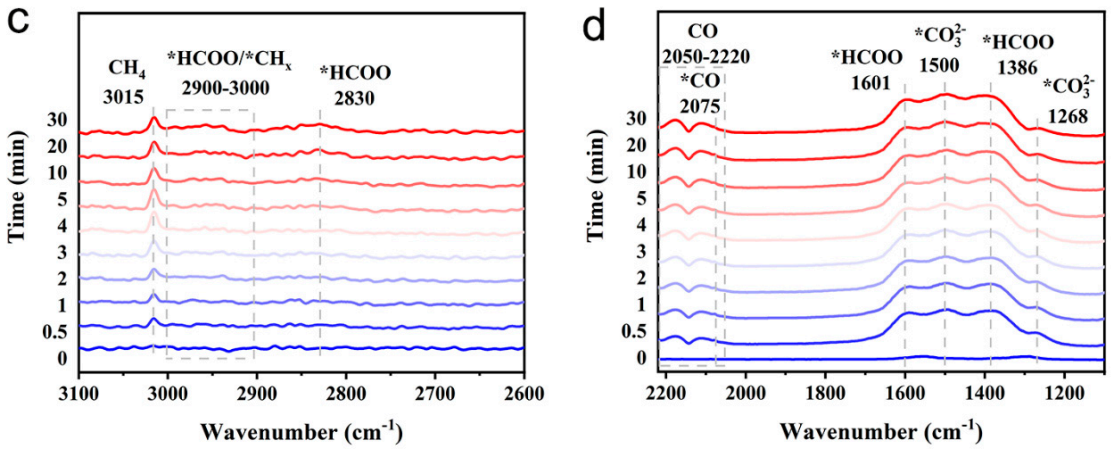

Figure 9. In situ CO_2 hydrogenation DRIFTS results of (**a**,**b**) $KFMM_0$ and (**c**,**d**) $KFMM_{0.15}$ catalysts. * represented adsorbed species.

3. Experimental Section

3.1. Catalyst Preparation

A series of $KFMM_x$ (KFMM is an abbreviation of KFeMnMg) catalysts were synthesized by a coprecipitation method, where x (varies from 0 to 0.20) represents the atomic ratio of Mg in metal elements. In total, 16.9 mmol $FeCl_3{\cdot}6H_2O$, 9.2 mmol $FeCl_2{\cdot}4H_2O$, 7.8 mmol $MnCl_2{\cdot}4H_2O$, 14.5 mmol $MgCl_2{\cdot}6H_2O$, and hydrochloric acid were dissolved in 20 mL of deionized water, which was called solution A. 0.4 mol KOH was dissolved in 250 mL of deionized water to form solution B. Solution A was added into solution B with stirring at 50 °C. After 3 h of stirring, the product was washed with a large amount of deionized water and dried at 100 °C overnight to obtain FMM_x. Then, K_2CO_3 was dissolved in an appropriate amount of deionized water (according to the saturated water adsorption of FMM_x). FMM_x was added to the above solution and stirred for 24 h. The suspension was dried at 100 °C overnight and calcined in N_2 at 350 °C for 3 h to obtain $KFMM_x$. The weight percentage of K was fixed at 3%.

PDVB was synthesized according to the reported method [31]. In total, 0.5 g of azobisisobutyronitrile (AIBN) was added to 10 g of divinylbenzene (DVB) and stirred at room temperature for 1 h. Then, the solution was transferred to a reactor and heat-treated at 100 °C for 24 h. The obtained solids were washed with methanol and then dried at 100 °C for 8 h to prepare PDVB. The composite catalysts were typically prepared by the physical mixing of $KFMM_x$ and PDVB with a mass ratio of 1:1, including powder mixing (donated as $KFMM_x$/PDVB-P), granule mixing (donated as $KFMM_x$/PDVB-G) and mortar mixing (donated as $KFMM_x$/PDVB-M).

3.2. Catalyst Characterization

The N_2 adsorption–desorption isotherms were determined by the JW-BK100B-specific surface analyzer. The morphology of the catalyst was characterized by the MIRA 3 LMH mode field emission scanning electron microscope (SEM) and FEI Talos F200X transmission electron microscope (TEM). Before characterization, the sample was dispersed in ethanol and then deposited on a carbon film. The X-ray diffraction (XRD) patterns of $KFMM_x$ were carried out on the Rigaku Ultima IV X-ray diffractometer with the Cu target (40 mV, 40 mA). The contact angle (CA) tests were taken on a POWEREACH JC2000C contact angle measuring instrument. Before the test, the catalyst was pressed, and then a 50 μL injector was used to drop demineralized water to test the contact angle between the water and the catalyst. Fourier-transform infrared spectroscopy (FT-IR) was used to analyze the phase composition and structure of PDVB and was taken by the Nicolet™ iS50 instrument with a DTGS detector. X-ray photoelectron spectroscopy (XPS) was carried out by using an

ESCALAB250Xi X-ray photoelectron spectrometer equipped with an Al K_α (1486.6 eV) quartz monochrometer source.

H_2 temperature-programmed reduction (H_2-TPR), H_2 temperature-programmed desorption (H_2-TPD), and CO_2 temperature-programmed desorption (CO_2-TPD) experiments were tested on a DAS-7000 instrument with a TCD detector. As for the H_2-TPR test, the catalysts were first cleaned by He at 350 °C for 1 h. After that, the samples were cooled to 50 °C and injected with a 10% H_2/Ar mixture (50 mL/min) for 0.5 h. After baseline stabilization, the samples were heated up to 800 °C at 10 °C/min. As for H_2-TPD and CO_2-TPD tests, catalysts were firstly reduced by 10% H_2/He at 350 °C for 1 h and purged by He for 1 h. After cooling down to 50 °C, the catalysts were treated with 10% H_2/He or 10% CO_2/He for 1 h; then, He was introduced for 1h to remove the weak physically adsorbed H_2 or CO_2 on the surface. The desorption was performed by heating from 50 °C to 600 °C. In situ diffuse reflection infrared Fourier transform spectroscopy (in situ DRIFTS) was tested using the Nicolet™ iS50 instrument with an MCT detector. The catalysts were first reduced in pure H_2 at 350 °C for 1 h and purged in Ar for 1 h. The background spectra were collected by 32 scans at a resolution of 4 cm^{-1} after cooling down to 320 °C in Ar flow. The DRIFTS tests were carried out at 320 °C in a CO_2/H_2 (1:3 by volume) flow at 1 MPa.

3.3. Catalyst Activity Test

The CO_2 hydrogenation reaction over the $KFMM_x$ and $KFMM_x$/PDVB composite catalysts was carried out in a fixed-bed reactor. Before the reaction, 0.5 g of the catalyst was treated with pure H_2 at 350 °C for 8 h and reactant gas (CO_2:H_2:N_2 = 10:39:51) was then fed in at a temperature of 320~340 °C and a weighted hourly space velocity (WHSV) of 2000~4000 mL/(g_{cat}·h) as the system was pressurized to 3 MPa. The water was added by a peristaltic pump and heated to 150 °C to form steam. All products were heated to 150 °C and analyzed by online gas chromatography (GC2060), where N_2, CO, CH_4, and CO_2 were detected by a thermal conducted detector (TCD), and hydrocarbons were detected by two flame ionization detectors (FIDs). CO_2 conversion and product selectivity were calculated according to the full product analysis. The carbon balance of all catalysts was between 96 and 97%.

4. Conclusions

According to the present composition of power plant flue gas, we prepared multifunctional $KFMM_x$/PDVB catalysts for H_2O-containing low-concentration CO_2 hydrogenation to produce light olefins. The optimized $KFMM_{0.15}$ catalyst achieved a light olefin yield of 6.22%, which was 38.8% higher than that without the Mg catalyst in low-concentration CO_2 hydrogenation. Several characterization results confirmed that the Mg promoter played critical roles in regulating the adsorption capacity of CO_2, increasing the surface electron density of Fe species, and promoting the formation of iron carbide active sites. The introduction of water steam in feed gas was found to weaken the catalytic performance severely. In response, the optimized $KFMM_{0.15}$/PDVB-P multifunctional catalyst exhibited a light olefin yield of 5.47%, which was 36.9% higher than that of the sole $KFMM_{0.15}$ catalyst in H_2O-containing CO_2 hydrogenation. The structural characterization results proved that water steam could oxidize the Fe_5C_2 active phase, thus severely reducing the catalytic performance, while the introduction of hydrophobic PDVB weakened the negative effect to some extent. Note that the distance between $KFMM_{0.15}$ and PDVB greatly affected the catalytic performance of the multifunctional catalyst, which could be reasoned by the balance of the H_2O removal rate and Fe_5C_2 formation. It benefited from the rational design of the catalyst, indicating how our multifunctional Fe-based catalyst shows great potential for practical application in CO_2 utilization.

Author Contributions: L.F. and S.G. carried out the synthesis, catalytic test, and characterization of the catalysts. Z.Y., Y.C., J.M., X.S., Q.C., X.Z. and G.W. participated in the investigation of synthesis. L.F. wrote the manuscript text with the assistance of D.X. and M.D. All authors have read and agreed to the published version of the manuscript.

Funding: This research was funded by [Study on catalyst and process for light olefins synthesis from carbon dioxide in flue gas of power plant] grant number [CY790000JS20220235] And The APC was funded by [Study on catalyst and process for light olefins synthesis from carbon dioxide in flue gas of power plant].

Data Availability Statement: All the data can be found in the manuscript.

Conflicts of Interest: The authors declare no competing financial interest.

References

1. National Oceanic & Atmospheric Administration. *Carbon Cycle Greenhouse Gases—Trends in Atmospheric Carbon Dioxide*; Global Monitoring Laboratory Earth System Research Laboratories: Boulder, CO, USA, 2024. Available online: https://gml.noaa.gov/ccgg/trends/mlo.html (accessed on 5 February 2024).
2. IPCC. *AR4 Climate Change 2007: Impacts, Adaptation, and Vulnerability—IPCC*; IPCC: Geneva, Switzerland, 2007. Available online: https://www.ipcc.ch/report/ar4/wg2/ (accessed on 5 February 2024).
3. Aresta, M.; Dibenedetto, A.; Angelini, A. Catalysis for the Valorization of Exhaust Carbon: From CO_2 to Chemicals, Materials, and Fuels. Technological Use of CO_2. *Chem. Rev.* **2013**, *114*, 1709–1742. [CrossRef]
4. Galvis, H.M.T.; de Jong, K.P. Catalysts for Production of Lower Olefins from Synthesis Gas: A Review. *ACS Catal.* **2013**, *3*, 2130–2149. [CrossRef]
5. Galvis, H.M.T.; Bitter, J.H.; Khare, C.B.; Ruitenbeek, M.; Dugulan, A.I.; de Jong, K.P. Supported Iron Nanoparticles as Catalysts for Sustainable Production of Lower Olefins. *Science* **2012**, *335*, 835–838. [CrossRef] [PubMed]
6. Zhong, L.; Yu, F.; An, Y.; Zhao, Y.; Sun, Y.; Li, Z.; Lin, T.; Lin, Y.; Qi, X.; Dai, Y.; et al. Cobalt Carbide Nanoprisms for Direct Production of Lower Olefins from Syngas. *Nature* **2016**, *538*, 84–87. [CrossRef]
7. Yang, Q.; Kondratenko, V.A.; Petrov, S.A.; Doronkin, D.E.; Saraçi, E.; Lund, H.; Arinchtein, A.; Kraehnert, R.; Skrypnik, A.S.; Matvienko, A.A.; et al. Identifying Performance Descriptors in CO_2 Hydrogenation over Iron-Based Catalysts Promoted with Alkali Metals. *Angew. Chem. Int. Ed.* **2022**, *61*, e202116517. [CrossRef] [PubMed]
8. Li, W.; Wang, H.; Jiang, X.; Zhu, J.; Liu, Z.; Guo, X.; Song, C. A Short Review of Recent Advances in CO_2 Hydrogenation to Hydrocarbons over Heterogeneous Catalysts. *RSC Adv.* **2018**, *8*, 7651–7669. [CrossRef] [PubMed]
9. Wang, D.; Xie, Z.; Porosoff, M.D.; Chen, J.G. Recent Advances in Carbon Dioxide Hydrogenation to Produce Olefins and Aromatics. *Chem* **2021**, *7*, 2277–2311. [CrossRef]
10. Guo, L.; Sun, J.; Ge, Q.; Tsubaki, N. Recent Advances in Direct Catalytic Hydrogenation of Carbon Dioxide to Valuable C_{2+} Hydrocarbons. *J. Mater. Chem. A* **2018**, *6*, 23244–23262. [CrossRef]
11. Orege, J.I.; Wei, J.; Han, Y.; Yang, M.; Sun, X.; Zhang, J.; Amoo, C.C.; Ge, Q.; Sun, J. Highly Stable Sr and Na Co-Decorated Fe Catalyst for High-Valued Olefin Synthesis from CO_2 Hydrogenation. *Appl. Catal. B Environ.* **2022**, *316*, 121640. [CrossRef]
12. Xu, Y.; Zhai, P.; Deng, Y.; Xie, J.; Liu, X.; Wang, S.; Ma, D. Highly Selective Olefin Production from CO_2 Hydrogenation on Iron Catalysts: A Subtle Synergy between Manganese and Sodium Additives. *Angew. Chem.* **2020**, *59*, 21736–21744. [CrossRef]
13. Yang, C.; Zhao, H.; Hou, Y.; Ma, D. Fe_5C_2 Nanoparticles: A Facile Bromide-Induced Synthesis and as an Active Phase for Fischer–Tropsch Synthesis. *J. Am. Chem. Soc.* **2012**, *134*, 15814–15821. [CrossRef] [PubMed]
14. Chang, Q.; Zhang, C.; Liu, C.; Wei, Y.; Cheruvathur, A.V.; Dugulan, A.I.; Niemantsverdriet, J.W.; Liu, X.; He, Y.; Qing, M.; et al. Relationship between Iron Carbide Phases (ε-Fe_2C, Fe_7C_3, and χ-Fe_5C_2) and Catalytic Performances of Fe/SiO_2 Fischer–Tropsch Catalysts. *ACS Catal.* **2018**, *8*, 3304–3316. [CrossRef]
15. Bukur, D.B.; Todic, B.; Elbashir, N. Role of Water-Gas-Shift Reaction in Fischer–Tropsch Synthesis on Iron Catalysts: A Review. *Catal. Today* **2016**, *275*, 66–75. [CrossRef]
16. de Smit, E.; Cinquini, F.; Beale, A.M.; Safonova, O.V.; van Beek, W.; Sautet, P.; Weckhuysen, B.M. Stability and Reactivity of $\epsilon-\chi-\theta$ Iron Carbide Catalyst Phases in Fischer−Tropsch Synthesis: Controlling μ_C. *J. Am. Chem. Soc.* **2010**, *132*, 14928–14941. [CrossRef] [PubMed]
17. Zhang, Z.; Chen, B.; Jia, L.; Liu, W.; Gao, X.; Gao, J.; Meng, B.; Tan, Y.; He, Y.; Tu, W.; et al. Unraveling the Role of Fe_5c_2 in CH_4 Formation during CO_2 Hydrogenation over Hydrophobic Iron Catalysts. *Appl. Catal. B Environ.* **2023**, *327*, 122449. [CrossRef]
18. Xu, Y.; Li, X.; Gao, J.; Wang, J.; Ma, G.; Wen, X.; Yang, Y.; Li, Y.; Ding, M. A Hydrophobic FeMn@Si Catalyst Increases Olefins from Syngas by Suppressing C1 By-Products. *Science* **2021**, *371*, 610–613. [CrossRef]
19. Javed, M.; Zhang, G.; Gao, W.; Cao, Y.; Dai, P.; Ji, X.; Lu, C.; Yang, R.; Xing, C.; Sun, J. From Hydrophilic to Hydrophobic: A Promising Approach to Tackle High CO_2 Selectivity of Fe-Based Fischer-Tropsch Microcapsule Catalysts. *Catal. Today* **2019**, *330*, 39–45. [CrossRef]
20. Anderson, K.; Peters, G. The Trouble with Negative Emissions. *Science* **2016**, *354*, 182–183. [CrossRef]
21. Davis, S.J.; Socolow, R.H. Commitment Accounting of CO_2 Emissions. *Environ. Res. Lett.* **2014**, *9*, 084018. [CrossRef]

22. Voumik, L.C.; Islam, M.A.; Ray, S.; Mohamed Yusop, N.Y.; Ridzuan, A.R. CO_2 Emissions from Renewable and Non-Renewable Electricity Generation Sources in the G7 Countries: Static and Dynamic Panel Assessment. *Energies* **2023**, *16*, 1044. [CrossRef]
23. Thitakamol, B.; Veawab, A.; Aroonwilas, A. Environmental Impacts of Absorption-Based CO_2 Capture Unit for Post-Combustion Treatment of Flue Gas from Coal-Fired Power Plant. *Int. J. Greenh. Gas Control* **2007**, *1*, 318–342. [CrossRef]
24. Chapel, D.; Ernest, J.; Mariz, C. *Recovery of CO_2 from Flue Gases: Commercial Trends*; Canadian Society of Chemical Engineers Annual Meeting: Saskatoon, SK, Canada, 1999.
25. Aslam, A.; Thomas-Hall, S.R.; Mughal, T.; Zaman, Q.; Ehsan, N.; Javied, S.; Schenk, P.M. Heavy Metal Bioremediation of Coal-Fired Flue Gas Using Microalgae under Different CO_2 Concentrations. *J. Environ. Manag.* **2019**, *241*, 243–250. [CrossRef]
26. Ramasubramanian, K.; Verweij, H.; Winston Ho, W.S. Membrane Processes for Carbon Capture from Coal-Fired Power Plant Flue Gas: A Modeling and Cost Study. *J. Membr. Sci.* **2012**, *421–422*, 299–310. [CrossRef]
27. Fu, L.; Ren, Z.; Si, W.; Ma, Q.; Huang, W.; Liao, K.; Huang, Z.; Wang, Y.; Li, J.; Xu, P. Research Progress on CO_2 Capture and Utilization Technology. *J. CO2 Util.* **2022**, *66*, 102260. [CrossRef]
28. Wang, X.; Song, C. Carbon Capture from Flue Gas and the Atmosphere: A Perspective. *Front. Energy Res.* **2020**, *8*, 560849. [CrossRef]
29. Yu, G.; Sun, B.; Pei, Y.; Xie, S.; Yan, S.; Qiao, M.; Fan, K.; Zhang, X.; Zong, B. Fe_xO_y@C Spheres as an Excellent Catalyst for Fischer−Tropsch Synthesis. *J. Am. Chem. Soc.* **2009**, *132*, 935–937. [CrossRef] [PubMed]
30. Zhu, J.; Wang, P.; Zhang, X.; Zhang, G.; Li, R.; Li, W.; Senftle, T.P.; Liu, W.; Wang, J.; Wang, Y.; et al. Dynamic Structural Evolution of Iron Catalysts Involving Competitive Oxidation and Carburization during CO $_2$ Hydrogenation. *Sci. Adv.* **2022**, *8*, eabm3629. [CrossRef]
31. Fang, W.; Wang, C.; Liu, Z.; Wang, L.; Liu, L.; Li, H.; Xu, S.; Zheng, A.; Qin, X.; Liu, L.; et al. Physical Mixing of a Catalyst and a Hydrophobic Polymer Promotes CO Hydrogenation through Dehydration. *Science* **2022**, *377*, 406–410. [CrossRef]
32. Lu, F.; Chen, X.; Wang, W.; Zhang, Y. Adjusting the CO_2 Hydrogenation Pathway via the Synergic Effects of Iron Carbides and Iron Oxides. *Catal. Sci. Technol.* **2021**, *11*, 7694–7703. [CrossRef]
33. Martín, N.; Cirujano, F.G. Multifunctional Heterogeneous Catalysts for the Tandem CO_2 Hydrogenation-Fischer Tropsch Synthesis of Gasoline. *J. CO2 Util.* **2022**, *65*, 102176. [CrossRef]
34. Zhai, P.; Xu, C.; Gao, R.; Liu, X.; Li, M.; Li, W.-X.; Fu, X.-P.; Jia, C.-J.; Xie, J.; Zhao, M.; et al. Highly Tunable Selectivity for Syngas-Derived Alkenes over Zinc and Sodium-Modulated Fe_5c_2 Catalyst. *Angew. Chem.* **2016**, *55*, 9902–9907. [CrossRef] [PubMed]
35. Satthawong, R.; Koizumi, N.; Song, C.; Prasassarakich, P. Light Olefin Synthesis from CO_2 Hydrogenation over K-Promoted Fe–Co Bimetallic Catalysts. *Catal. Today* **2015**, *251*, 34–40. [CrossRef]
36. Cho, J.M.; Kim, B.-G.; Han, G.Y.; Sun, J.; Jeong, H.-K.; Bae, J.W. Effects of Metal-Organic Framework-Derived Iron Carbide Phases for CO Hydrogenation Activity to Hydrocarbons. *Fuel* **2020**, *281*, 118779. [CrossRef]
37. Heyl, D.; Rodemerck, U.; Bentrup, U. Mechanistic Study of Low-Temperature CO_2 Hydrogenation over Modified Rh/Al_2O_3 Catalysts. *ACS Catal.* **2016**, *6*, 6275–6284. [CrossRef]
38. Wang, X.; Shi, H.; Kwak, J.H.; Szanyi, J. Mechanism of CO_2 Hydrogenation on Pd/al_2O_3 Catalysts: Kinetics and Transient DRIFTS-MS Studies. *ACS Catal.* **2015**, *5*, 6337–6349. [CrossRef]
39. Tang, L.; Song, C.; Li, M.; Yang, X.; Hu, B. Study of K/Mn-MgO Supported Fe Catalysts with $Fe(CO)_5$and $Fe(NO_3)_3$as Precursors for CO Hydrogenation to Light Alkenes. *Chin. J. Chem.* **2013**, *31*, 1263–1268. [CrossRef]
40. de Araujo, J.C.S.; Sousa, C.B.A.; Oliveira, A.C.; Freire, F.N.A.; Ayala, A.P.; Oliveira, A.C. Dehydrogenation of Ethylbenzene with CO_2 to Produce Styrene over Fe-Containing Ceramic Composites. *Appl. Catal. A Gen.* **2010**, *377*, 55–63. [CrossRef]
41. Yang, R.; Zhang, Y.; Iwama, Y.; Tsubaki, N. Mechanistic Study of a New Low-Temperature Methanol Synthesis on Cu/MgO Catalysts. *Appl. Catal. A Gen.* **2005**, *288*, 126–133. [CrossRef]
42. Borchert, H.; Jürgens, B.; Zielasek, V.; Rupprechter, G.; Giorgio, S.; Henry, C.; Bäumer, M. Pd Nanoparticles with Highly Defined Structure on MgO as Model Catalysts: An FTIR Study of the Interaction with CO, O_2, and H_2 under Ambient Conditions. *J. Catal.* **2007**, *247*, 145–154. [CrossRef]
43. Xu, M.; Qin, X.; Xu, Y.; Zhang, X.; Zheng, L.; Liu, J.-X.; Wang, M.; Liu, X.; Ma, D. Boosting CO Hydrogenation towards c_{2+} Hydrocarbons over Interfacial TiO_{2-x}/Ni Catalysts. *Nat. Commun.* **2022**, *13*, 1–11. [CrossRef]
44. Galhardo, T.S.; Braga, A.H.; Arpini, B.H.; Szanyi, J.; Gonçalves, R.V.; Zornio, B.F.; Miranda, C.R.; Rossi, L.M. Optimizing Active Sites for High CO Selectivity during CO_2 Hydrogenation over Supported Nickel Catalysts. *J. Am. Chem. Soc.* **2021**, *143*, 4268–4280. [CrossRef]
45. Topsøe, N.-Y.; Topsøe, H. FTIR Studies of Dynamic Surface Structural Changes in Cu-Based Methanol Synthesis Catalysts. *J. Mol. Catal. A Chem.* **1999**, *141*, 95–105. [CrossRef]
46. Dandekar, A.; Vannice, M.A. Determination of the Dispersion and Surface Oxidation States of Supported Cu Catalysts. *J. Catal.* **1998**, *178*, 621–639. [CrossRef]
47. Zhao, K.; Wang, L.; Calizzi, M.; Moioli, E.; Züttel, A. In Situ Control of the Adsorption Species in CO_2 Hydrogenation: Determination of Intermediates and Byproducts. *J. Phys. Chem. C* **2018**, *122*, 20888–20893. [CrossRef]
48. Yanagisawa, Y.; Takaoka, K.; Yamabe, S.; Ito, T. Interaction of CO_2 with Magnesium Oxide Surfaces: A TPD, FTIR, and Cluster-Model Calculation Study. *J. Phys. Chem.* **1995**, *99*, 3704–3710. [CrossRef]

49. Yang, C.; Mu, R.; Wang, G.; Song, J.; Tian, H.; Zhao, Z.-J.; Gong, J. Hydroxyl-Mediated Ethanol Selectivity of CO_2 Hydrogenation. *Chem. Sci.* **2019**, *10*, 3161–3167. [CrossRef]
50. Bobadilla, L.F.; Santos, J.L.; Ivanova, S.; Odriozola, J.A.; Urakawa, A. Unravelling the Role of Oxygen Vacancies in the Mechanism of the Reverse Water–Gas Shift Reaction by *Operando* DRIFTS and Ultraviolet–Visible Spectroscopy. *ACS Catal.* **2018**, *8*, 7455–7467. [CrossRef]
51. Das, T.; Deo, G. Synthesis, Characterization and in Situ DRIFTS during the CO_2 Hydrogenation Reaction over Supported Cobalt Catalysts. *J. Mol. Catal. A Chem.* **2011**, *350*, 75–82. [CrossRef]